NAVAL POSTGRADUATE SCHOOL

MONTEREY, CALIFORNIA

THESIS

CREATION AND OPTIMIZATION OF NOVEL SOLAR CELL POWER VIA BIMATERIAL PIEZOELECTRIC MEMS DEVICE

by

David C. Baughman

December 2011

Thesis Advisor:	Dragoslav Grbovic
Second Reader:	Sebastian Osswald
Third Reader:	Daniel Bursch

Approved for public release; distribution is unlimited

THIS PAGE INTENTIONALLY LEFT BLANK

REPORT DOCUMENTATION PAGE			Form Approved OMB No. 0704–0188
Public reporting burden for this collection of information is estimated to average 1 hour per response, including the time for reviewing instruction, searching existing data sources, gathering and maintaining the data needed, and completing and reviewing the collection of information. Send comments regarding this burden estimate or any other aspect of this collection of information, including suggestions for reducing this burden, to Washington headquarters Services, Directorate for Information Operations and Reports, 1215 Jefferson Davis Highway, Suite 1204, Arlington, VA 22202–4302, and to the Office of Management and Budget, Paperwork Reduction Project (0704–0188) Washington DC 20503.			
1. AGENCY USE ONLY ***(Leave blank)***	**2. REPORT DATE** December 2011	**3. REPORT TYPE AND DATES COVERED** Master's Thesis	
4. TITLE AND SUBTITLE Creation and Optimization of Novel Solar Cell Power via Bimaterial Piezoelectric MEMS Device		**5. FUNDING NUMBERS**	
6. AUTHOR(S) David C. Baughman			
7. PERFORMING ORGANIZATION NAME(S) AND ADDRESS(ES) Naval Postgraduate School Monterey, CA 93943–5000		**8. PERFORMING ORGANIZATION REPORT NUMBER**	
9. SPONSORING /MONITORING AGENCY NAME(S) AND ADDRESS(ES) N/A		**10. SPONSORING/MONITORING AGENCY REPORT NUMBER**	
11. SUPPLEMENTARY NOTES The views expressed in this thesis are those of the author and do not reflect the official policy or position of the Department of Defense or the U.S. Government. IRB Protocol number ___N/A____.			
12a. DISTRIBUTION / AVAILABILITY STATEMENT Approved for public release; distribution is unlimited		**12b. DISTRIBUTION CODE** A	

13. ABSTRACT (maximum 200 words)

Current solar cell technology suffers low efficiencies in the commercial sector and cost prohibitive technology at higher efficiencies. This thesis investigates the possibility of a novel, alternate, avenue for the creation of solar power, which has the potential to be both cost effective and highly efficient. The approach converts solar energy into electrical energy via a MEMS device that utilizes spectrum-insensitive thermal absorption combined with power generation via the piezoelectric effect. The thesis investigates the underlying physics, materials needed, design requirements, computer modeling, optimization, and microfabrication process in the creation of such a device.

14. SUBJECT TERMS MEMS, piezoelectric, solar, energy, bimaterial, power			**15. NUMBER OF PAGES** 53
			16. PRICE CODE
17. SECURITY CLASSIFICATION OF REPORT Unclassified	**18. SECURITY CLASSIFICATION OF THIS PAGE** Unclassified	**19. SECURITY CLASSIFICATION OF ABSTRACT** Unclassified	**20. LIMITATION OF ABSTRACT** UU

NSN 7540–01–280–5500

Standard Form 298 (Rev. 8–98)
Prescribed by ANSI Std. Z39.18

THIS PAGE INTENTIONALLY LEFT BLANK

Approved for public release; distribution is unlimited

CREATION AND OPTIMIZATION OF NOVEL SOLAR CELL POWER VIA BIMATERIAL PIEZOELECTRIC MEMS DEVICE

David C. Baughman
Lieutenant Commander, United States Navy
Physics B.S., Mathematics B.S., United States Naval Academy, 2000
M.A., Naval War College, 2007

Submitted in partial fulfillment of the
requirements for the degree of

MASTER OF SCIENCE IN SPACE SYSTEMS OPERATIONS
and
MASTER OF SCIENCE IN PHYSICS

from the

NAVAL POSTGRADUATE SCHOOL
December 2011

Author: David C. Baughman

Approved by: Dragoslav Grbovic
Thesis Advisor

Sebastian Osswald
Second Reader

Daniel Bursch
Third Reader

Andres Larraza
Chair, Department of Physics

Rudy Panholzer
Chair, Space Systems Academic Group

THIS PAGE INTENTIONALLY LEFT BLANK

ABSTRACT

Current solar cell technology suffers low efficiencies in the commercial sector and cost prohibitive technology at higher efficiencies. This thesis investigates the possibility of a novel, alternate, avenue for the creation of solar power, which has the potential to be both cost effective and highly efficient. The approach converts solar energy into electrical energy via a MEMS device that utilizes spectrum-insensitive thermal absorption combined with power generation via the piezoelectric effect. The thesis investigates the underlying physics, materials needed, design requirements, computer modeling, optimization, and microfabrication process in the creation of such a device.

THIS PAGE INTENTIONALLY LEFT BLANK

TABLE OF CONTENTS

THIS PAGE INTENTIONALLY LEFT BLANK

LIST OF FIGURES

THIS PAGE INTENTIONALLY LEFT BLANK

ACKNOWLEDGMENTS

The author would like to thank his family, his advisors, the Space Systems Academic Group, the Physics Department, and the Naval Postgraduate School for their support in the completion of this thesis.

THIS PAGE INTENTIONALLY LEFT BLANK

I. INTRODUCTION

A. BACKGROUND

Due to current technological constraints, solar energy provides an untapped resource for use on the ground. Additionally, space assets suffer from extremely high overhead costs in order to use solar power at today's required efficiencies. If all solar energy that strikes the surface of the earth could be utilized, it would provide 6,000 times the current global consumption of primary energy, yet as of 2006 solar power represented less than 1% of electricity production from renewable sources [1]. The cause of this low percentage of use is due to the current cost of using solar power at reasonable efficiencies. Numerous efforts are underway to attempt to resolve this issue. Current avenues of solar research include photovoltaic, solar thermal devices, photosynthetic, photo(electro)chemical, thermal, and thermochemical processes. The most prevalent of these technologies, photovoltaic, suffers from the requirement of making efficient use of its semiconductor bandgap. This requirement inevitably leads to low efficiencies in the production of energy. In order to maximize this efficiency, the most advanced photovoltaic cells use different layered materials to maximize the bandgap energies for absorption. These multi-junction cells are cost prohibitive and still provide nominal beginning-of-life useful efficiencies of less than 30% [2].

B. NOVEL SOLAR CELL CREATION

This thesis therefore investigates the possibility of a novel, alternate, avenue for the utilization of solar power, which has the potential to be both cost effective and highly efficient. The novel approach to the conversion of solar energy into electrical energy incorporates a MEMS device, which utilizes a spectrum-insensitive thermal absorption of solar flux. This thermal energy is then

converted into mechanical energy via the thermal bimetallic effect and is converted once again into a useable electric potential via the piezoelectric effect. This MEMS device is then forced to oscillate via a heat sink, thereby generating a variable voltage and hence a pulsating current.

II. PHYSICS WITHIN THE DESIGN

Development of the proposed MEMS device incorporates numerous diverse concepts and physics integrated together. The five key concepts and physics required for this thesis are given below.

A. MICROELECTROMECHANICAL SYSTEMS

MEMS or MicroElectroMechanical Systems are devices or systems on the order of one to hundreds of microns in size and, as the name implies, comprise small electro-mechanical systems. MEMS is a growing field, includes diverse areas of research such as BioMEMS, Optical MEMS, Microfluidics, and Radio Frequency (RF) MEMS, and incorporates everyday devices such as the accelerometers found in phones and ink jet printer nozzles [3].

B. SOLAR ABSORPTION

As stated previously, current solar cells are highly dependent on the wavelength of light for their absorption of energy. In contrast to this, by making use of a thermal conversion process, the full spectrum of light can be utilized for energy absorption. The amount of energy gained in the thermal conversion process can be estimated by the temperature increase of the material, which is dependent on the ratio of solar absorptivity, α, and the IR emissivity, ε. This is highly beneficial for thermal conversion due to the fact that materials can be easily altered to create a desired ratio in order to achieve the needed temperature. To first order, this temperature is given by:

$$\sigma T^4 = (\alpha / \varepsilon) \times S \times (A_p / A) \tag{1}$$

where σ is the Stefan Boltzmann's constant, $5.67 \times 10^{-8} W / m^2 K^4$, A_p is the

projected area, A is the total area, and S is the solar constant (average of 1367 W/m^2 in space earth orbit and on average approximately 700 W/m^2 on the surface of the earth).

C. THERMAL EXPANSION

The thermal energy absorbed by the power generator element can be converted to mechanical energy via the thermal bimetallic effect. This process involves portions of the structure having two material layers, each having a different coefficient of thermal expansion, and tightly joined along their longitudinal axis. These materials serve as a single mechanical element such that when a thermal flux is applied, the element deforms. The beam bends toward the material with the lower coefficient of thermal expansion for a given temperature change. The deformation solely depends on the materials used and the thickness ratio [4]. The amount of deformation is given by [4]:

$$\theta = \frac{6(\Delta\alpha)(\Delta T)L}{t_1\left(\frac{(1+\lambda\xi)(1+\xi^3\lambda)+3\lambda\xi(\xi+1)^2}{\lambda\xi^2(\xi+1)}\right)} \tag{2}$$

where θ is the deformation vis-a-vis the free-end slope, Δα is the difference in the thermal expansion coefficients of the materials, ΔT is the temperature difference, L is the length of the element, t_1 is the thickness of the layer with the higher thermal expansion coefficient, λ is the ratio of Young's moduli between the two materials, and ξ is the thickness ratio between the two materials. It can be seen from Equation 2 that, to maximize the absorption, the two layers have to have materials with as large a difference in coefficients of thermal expansion as possible.

D. PIEZOELECTRIC EFFECT [3]

The final conversion from mechanical to electrical energy involves utilization of the piezoelectric effect. Discovered in 1880, this effect can produce a 1000 V/cm field from a 10^{-7} strain in piezoelectric materials such as quartz crystal. This effect is maximized in piezoelectric materials below the Curie point (and normally above 0 ℃) and varies for each material. The actual cause of the piezoelectric effect is the displacement of ionic charges within the crystal caused by the alteration of the spacing between the centers of charge sites in each domain cell. This effect occurs solely in noncentrosymmetric groups and is strongly orientation dependent. The customary polarization coincides with the z-axis of a rectangular coordinate system and is given by:

$$D_i = d_{ij} T_j + \varepsilon_{ik} E_k \tag{3}$$

where D is the electrical polarization and is given in each axis of a rectangular coordinate system by a 1 x 3 matrix, T is the applied mechanical stress and is a 1 x 6 matrix, d is the piezoelectric coefficient matrix and is a 6 x 3 matrix, ε is the electrical permittivity matrix and is a 3 x 3 matrix, and E is the electric field and is a 1 x 3 matrix. For the purpose of this thesis, since no electric field is being utilized to create the piezoelectric effect, the second term on the right can be left out and the equation reduces to $D_i = d_{ij} T_j$. D can be solved for by noting that the deformation given from Equation 2 is directly related to the strain and therefore the stress via the constitutive relation given by Hooke's law. The output voltage, V, is then related to the z component of D, defined by Equation 3, by the simple relation:

$$V = \frac{D_3 t}{\varepsilon} \tag{4}$$

where t is the thickness of the piezoelectric material in the z direction and ε is the permittivity of the material. Note that the principal polarization direction, 3, is the

only term utilized in this final equation since the contributions from components in other directions are negligible for piezoelectric materials polarized in the z direction.

E. CURRENT GENERATION

Due to the rapid rate of charge leakage that occurs in strained piezoelectric materials, generation of a continuous current for power utilization requires the voltage to oscillate [5]. In order to achieve this, a heat sink is placed near the maximal displacement of the MEMS device. The heat sink will lower the temperature of the MEMS device via thermal contact conduction until the MEMS device retracts a certain distance away from the heat sink. In general and in accordance with Fourier's law, the heat removed during this process is given by [6]:

$$Q = h\Delta TA \tag{5}$$

where Q is the heat flow, h is the thermal contact conductivity, A is the cross-sectional area, and ΔT is the temperature gradient in the direction of flow. However, it must be noted that this is a generalized approximation and not necessarily accurate due to the difficulties of accurately modeling the contact points between two solids. There are multiple competing analysis efforts that exist for thermal contact conductance and it is an active area of research.

The heat removal that occurs every time the device contacts the substrate will reduce the deformation of the device. The constant heat flux will then force the device back into contact with the substrate. This process will continue causing the MEMS device to reach an oscillatory motion and generate a continuous pulsating current.

III. MATERIALS SELECTION

One of the most important aspects to many MEMS applications is the selection of materials. The response to the physics noted above is dependent on both the operating environment and the materials utilized. This is especially important when noting the potential for utilization of these piezoelectric devices as solar cells in space where the temperature on the flux facing side of the solar cell in sun-synchronous orbit could be as high as 200 ℃ depending on the metal selected [7]. Due to the large difference in requirements for the materials utilized in space versus on the surface of the earth, two completely different material selection processes were conducted. However, the only difference in material selection between a ground-based unit and a space-based unit was determined to be in the piezoelectric materials. All other materials would be equally adequate for utilization in space as they would be on the surface.

A. PIEZOELECTRIC MATERIALS

The materials selection logically followed the criteria set forth in the physics and concepts described above. First and foremost, the piezoelectric material as well as the device as a whole, must be capable of being microfabricated with current MEMS manufacturing techniques. Second, the absorptivity and emissivity of the materials needed to be reviewed in order to ensure the solar flux would not heat the material to temperatures higher than desired. Third, the material needed to have high thermal conductivity in order to rapidly transfer thermal energy to a heat sink. The material also must have a low thermal expansion coefficient in order to ensure adequate bimorph thermal actuation when combined with the highly-thermally-expansive layer. Fourth, the material must have adequate piezoelectric properties for high efficiencies of

energy conversion. Finally, the specific needs given by the harshness of space required that the material chosen for space be stable, strong, hard, non-reactive, and shock resistant.

1. Aluminum Nitride (AlN)

AlN was the piezoelectric material chosen for development of the solar MEMS device for use on the surface of the earth. AlN is a large band gap (6 eV) made of a wurtzite crystal structure with a large resistivity and is perfectly compatible with current silicon technology [8]. Many methods for growth of AlN exist including chemical vapor deposition (CVD), molecular beam epitaxy, ion beam nitridation, laser-ablation, and reactive sputtering [9]. Additionally, the successful growth of AlN for laboratory purposes is facilitated by the fact that sputtered AlN maintains its piezoelectric properties with growth up to 10° offset from normal without losing the functionality of the piezoelectric layer [10]. The solar absorption of AlN is also respectable with the absorptivity to emissivity ratio of 1 being utilized for this thesis [11], [12]. The thermal conductivity of AlN is high with a measured value of single crystal AlN of 2.85 W/(cm℃) at 27 ℃ and the thermal expansion coefficient is low having a value of $5.27\times10^{-6}C^{-1}$ measured at 27 ℃ [13], [14]. AlN, which demonstrates moderately good piezoelectric properties, has been shown to have no deviation in its piezoelectric constants up to 300 ℃ and only slight alteration is expected up to a temperature of 1150 ℃ [10]. In summary, AlN is a highly stable, non-reactive piezoelectric material that exhibits the desired properties for the solar MEMS device.

2. Silicon Carbide (SiC)

Silicon Carbide exists in over 100 different modifications all with the same stoichiometry. The polytypes of SiC exist as a combination of hexagonal and cubic bilayers with the 6H or Six Hexagonal structure being the one selected for this thesis since it is the easiest to prepare on an SiC substrate and has been

studied greatly [15]. Like AlN, SiC (6H) is also composed of a wurtzite crystal structure, but unlike AlN has a repeated stacking sequence of ABCACB. The growth of SiC is well established and many techniques exist including sublimation, high-temperature chemical vapor deposition (HTCVD), and epitaxy [16]. Similar values to AlN exist for SiC for its absorptivity to emissivity ratio and so the ratio value utilized for this thesis was 1 [17], [18]. The thermal conductivity of SiC (6H) is high with a measured value of 4.9 W/(cm℃) and the thermal expansion coefficient is extremely small with a value of $4.3\times10^{-6}{}^{\circ}C^{-1}$ measured at 27 ℃ [19], [20]. The other polytypes of SiC, including 3C-SiC exhibit similar thermal properties. Although the piezoelectric properties of SiC are not as promising as AlN, they are still acceptable as the modeling conducted in this thesis demonstrates. Additionally, there is the potential for SiC-AlN combinations when utilizing 3C-SiC (which is not a wurtzite) in order to combine the piezoelectric properties of AlN with the strain gauge properties of SiC [10]. This would also benefit growth on a Si substrate vice a SiC substrate. In addition to the above attributes, SiC is an ideal candidate for space applications due to its extremely high fracture toughness (3–4 times greater than silicon) and its high ability to withstand irradiation [10], [21].

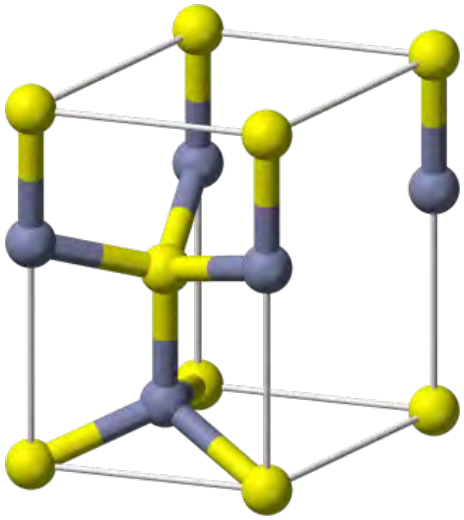

Figure 1: Wurtzite unit cell; grey balls represent metal atoms (From "Wurtzite unit cell," Wikipedia, 2007)

B. BIMATERIAL

Aluminum (Al) is an abundant, lightweight material with a high resistance to corrosion. Research has shown that it offers high performance as a thermal bimaterial actuator due to its high coefficient of thermal expansion and so it was a natural choice for the bimaterial in this thesis [4]. Al's thermal conductivity is extremely high with a value of 237 W/(mK) at 27 ℃ and its thermal expansion coefficient is very high as well with a value of $23.1\times10^{-6}{}^{\circ}C^{-1}$ at 25 ℃ [22].

C. SUBSTRATE

The substrate utilized serves two primary functions. First, it must be able to act as a heat sink when it comes into contact with the MEMS solar device. In order to accomplish this, the material must have a high thermal conductivity and a low coefficient of thermal expansion. Second, the heat sink will act as the base on which to build the Solar MEMS device. Therefore, current techniques for growth on the heat sink substrate must exist. Processes for growing thin films of both AlN and SiC exist for growth on both Si and SiC substrates therefore they are both potential candidates as heat sinks. Additionally, Si has a very high

thermal conductivity value of 156 W/(mK) at 27 ℃ and a very low coefficient of thermal expansion value of $2.616\times10^{-6}°C^{-1}$ at 27 ℃ making it a feasible option as an initial heat sink for study in this thesis [23]. Unfortunately, SiC's thermal conductivity value is much too low to be a viable option as a heat sink. However, a graphene layer, with a reported thermal conductivity value of 3080–5000 W/(mK) [24], has been grown on SiC substrates via epitaxial growth on top of a thin sputtered layer of AlN [25]. In a feasibility study conducted by S. Subrina et al in 2009 at the University of California Riverside, a layer of graphene effectively acted as a heat spreader, substantially lowering localized hot spot temperature values [24]. Therefore, the possibility exists to utilize SiC as an effective substrate allowing for the additional fabrication requirement of adding a graphene layer in order to ensure an effective heat sink.

THIS PAGE INTENTIONALLY LEFT BLANK

IV. DESIGN

A. BIMATERIAL DESIGN

In order to maximize the displacement of the bimaterial, the optimal thickness has been shown to be [4]:

$$\xi_{opt} = \frac{1}{\sqrt{\lambda}} \tag{6}$$

where ξ_{opt} is the optimal thickness ratio and λ is given by the ratio of Young's moduli from Equation 2. For the case of AlN and Al, utilizing the Young's moduli 308 GPa and 70 GPa respectively, this value is 2.09 [26], [27]. For SiC and Al utilizing the Young's moduli 748 GPa and 70 GPa, respectively, this value is 3.26 [28], [27]. Figure 2 demonstrates thickness optimization for the case of AlN and Al. The images show the steady state solution of four different cases utilizing COMSOL Multiphysics software. In these cases, the relative thicknesses were altered while keeping all other variable including heat flux, total thickness, and length constant. The maximum deflection is seen to occur in Figure 2.iii where the ratio used was the optimal ratio solved for above. In Figure 3, it can be seen that by changing the AlN to SiC, the optimal ratio for AlN and Al no longer provides the maximum deflection. Figure3.ii shows the maximum deflection for SiC and Al, which is equal to the above solved for ratio of 3.26.

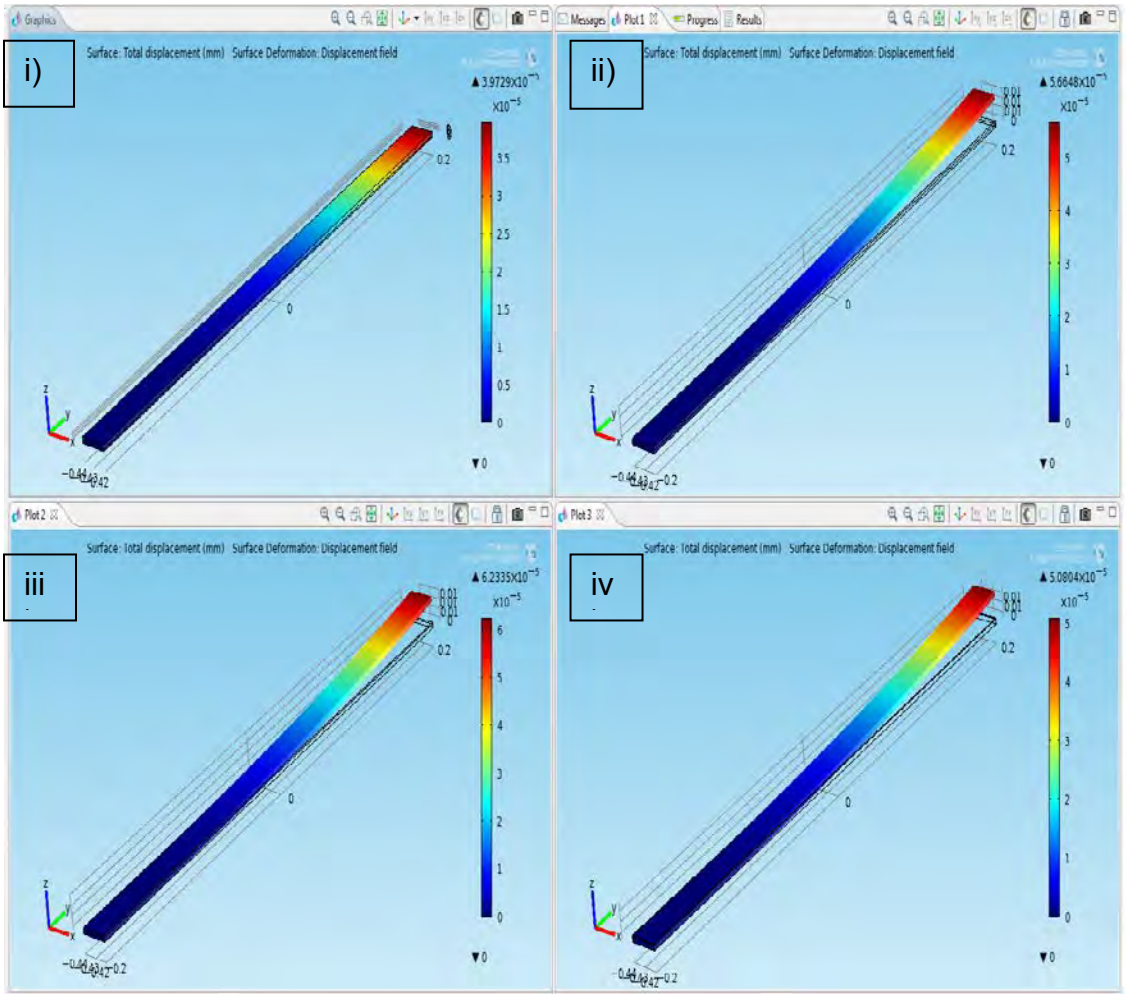

Figure 2: **Al and Al bimaterial thickness optimization (thickness ratios are in microns): i) 2–1 ii) 1.5–1.5 iii) 1–2 iv) 2.5-**

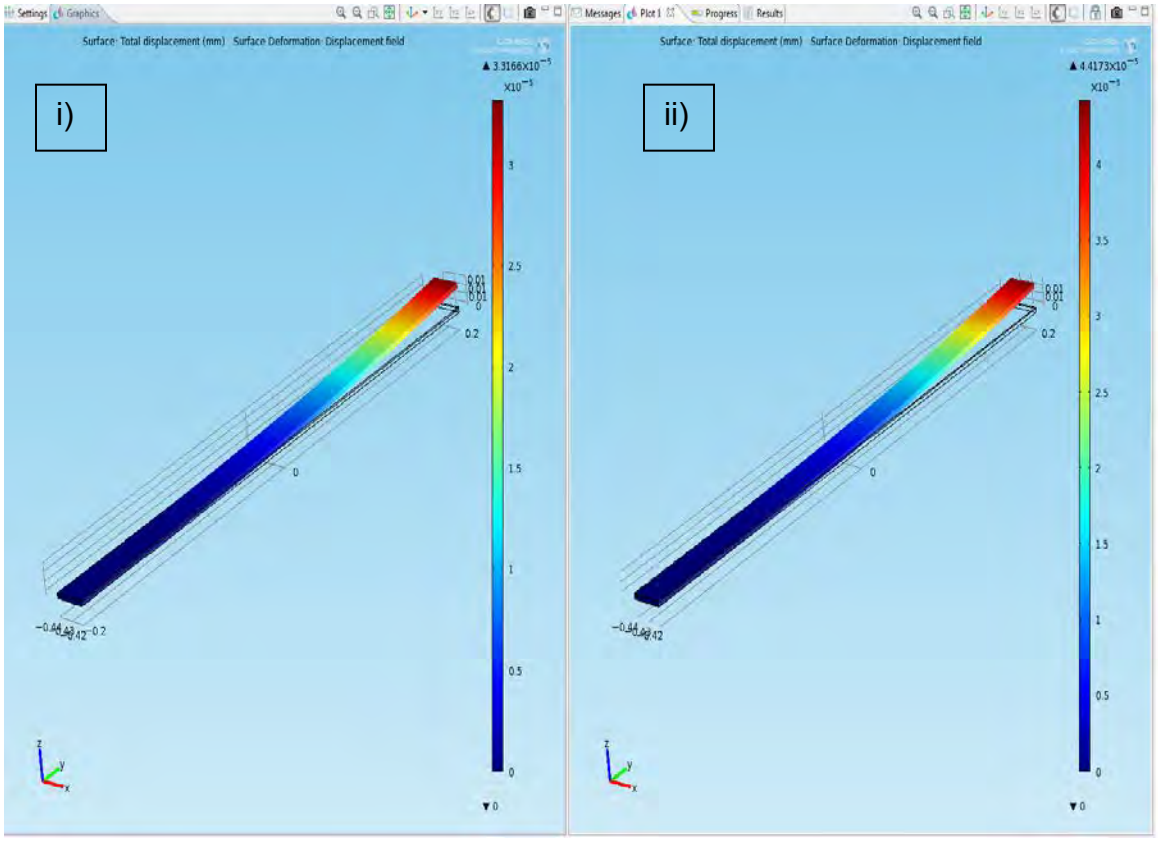

Figure 3: SiC and Al Bimaterial thickness optimization (thickness ratios are given):i)1–2 ii)1–3.2

B. GENERAL DIMENSIONS

Current microfabrication techniques provide a standard thin film deposition of MEMS materials of between 1–10 microns deposited on a substrate. Additionally, from Equation 2, it can readily be noticed that the angle of deformation is proportional to the length of the bimaterial and inversely proportional to the thickness. Based on the microfabrication constraint noted above as well as the desire to maximize the length to thickness ratio, a thickness of 1 micron was utilized for the piezoelectric material and 2 microns for thermal bimaterial in this thesis. The maximal amount of voltage could be produced if the bimorph were infinitely long and infinitely thin. This is obviously unrealistic, but larger displacements can be realized by creating multifold arms thereby simulating a longer arm length. Multifold arms utilize alternating bimaterial layers in order to increase the deformation on each subsequent leg [29]. Utilizing COMSOL Multiphysics modeling, the multifold arm effect is demonstrated in Figure 4. In each of the four cases demonstrated in Figure 4, the heat flux and dimensions of the legs were held constant. Figure 4.ii demonstrates how adding the bimaterial to every leg does not greatly benefit the total displacement of the multifold arms due to the fact that the bimaterials angle of deflection is almost equivalent on each end of each respective leg. The angle of deformations are cumulative ($\theta_1 + \theta_2 + ... = \theta_{total}$) for each alternating leg and due to the increase in temperature of each leg further from the fixed edge, each subsequent angle is larger than the last in accordance with Equation 2. The displacement in Figure 4.iii is 42.36 times as great as Figure 4.i and the displacement in Figure 4.iv is 641.8 times as great as Figure 4.i. An even greater effect is gained by alternating the placement of the bimaterial between the top and bottom of the piezoelectric material creating a “flip-over” leg structure, but limitations in current microfabrication techniques prohibit this technique [29]. In order to ensure compliance with current microfabrication capabilities, the solar MEMS device will

place the piezoelectric layer fewer than 10 microns above the heat sink. Therefore, it was determined that three bimaterial multifold arms would be utilized, each 400 microns long and 20 microns wide. In accordance with the multifold design described above, a piezoelectric leg of the same dimensions will be placed between each bimaterial leg.

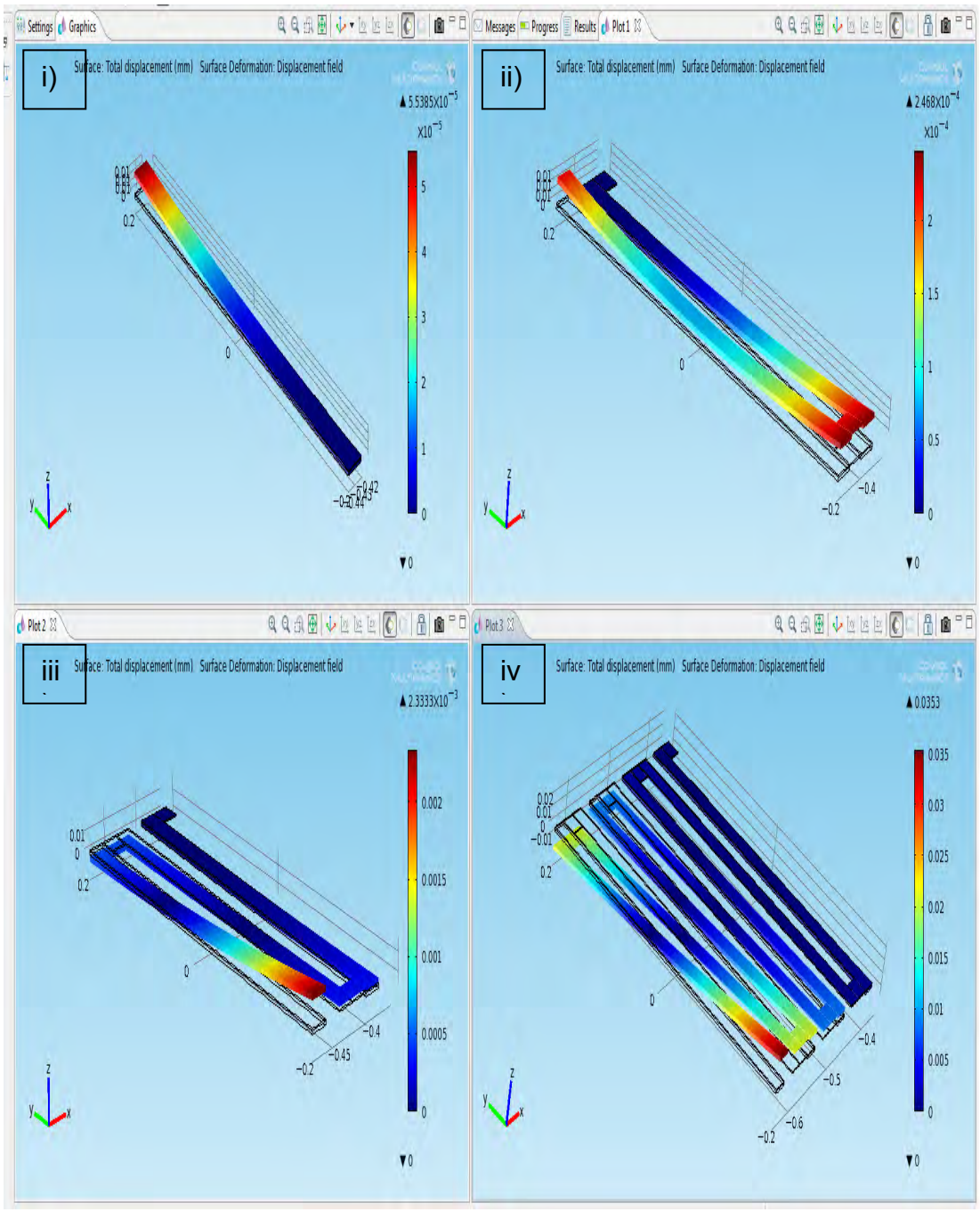

Figure 4: Effect of multifold arms to total displacement

C. REMOVAL OF HEAT

As previously discussed, the bending of the multifold arms must have a method of heat removal in order to cause the MEMS device to fluctuate and force an oscillatory motion in the device. In order to maximize this in accordance with Equation 5, a large center pad of piezoelectric material will be placed between two identical sets of multifold arms. The pad can also improve the absorptive area of the device in order to maximize the incoming heat flux. The pads dimensions are 460 microns wide by 320 microns long and are designed so as to also create an easily machineable structure.

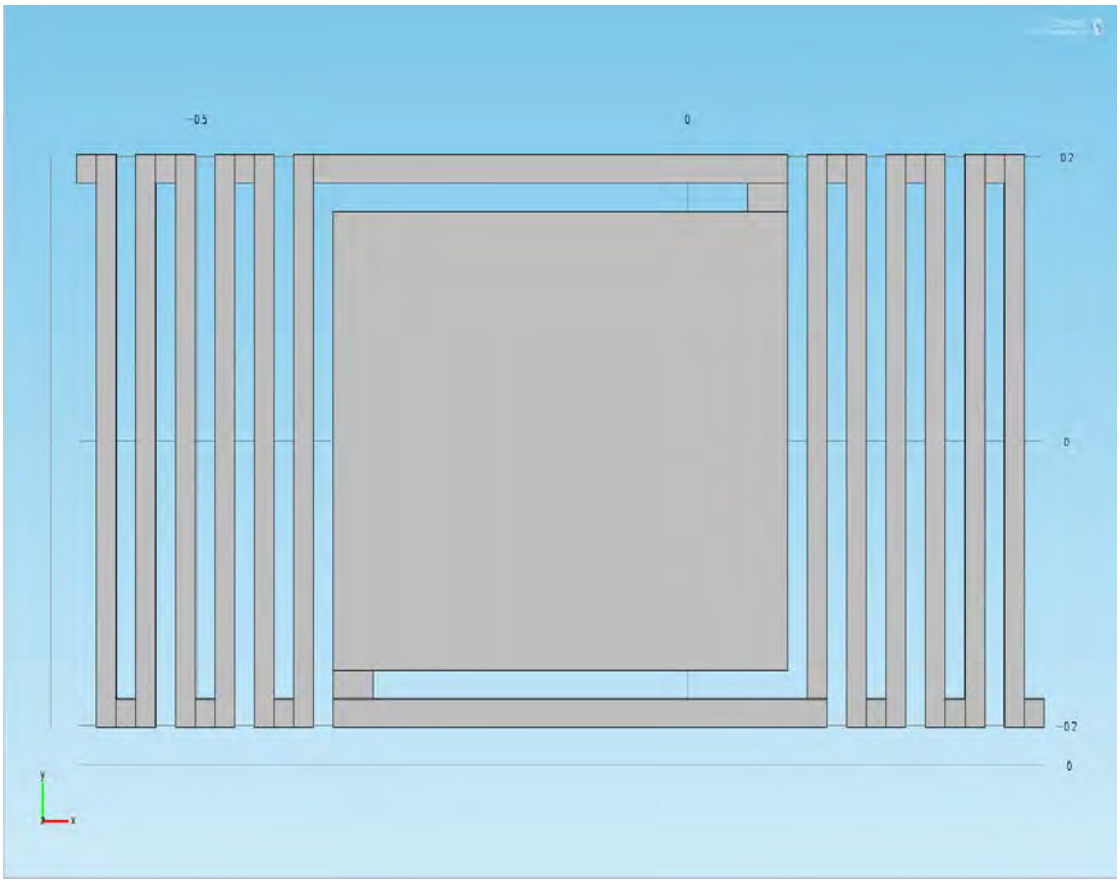

Figure 5: Solar MEMS device

D. INITIAL DESIGN

The initial design placed the Al material toward the incident heat flux with the alternating legs placed so as to lower the center pad with legs toward the heat sink (see Figure 5). Long cross legs were placed in order to minimize the shear stresses on the center pad. This design was not effective as the innermost legs displacement was greater than the center pad. This indicated the strong possibility that the center pad may never touch the substrate. Additionally, due to the torque created by the innermost bimaterial legs attachment to the center pad, the center pad's deformation was not uniform as can be seen by Figure 6.

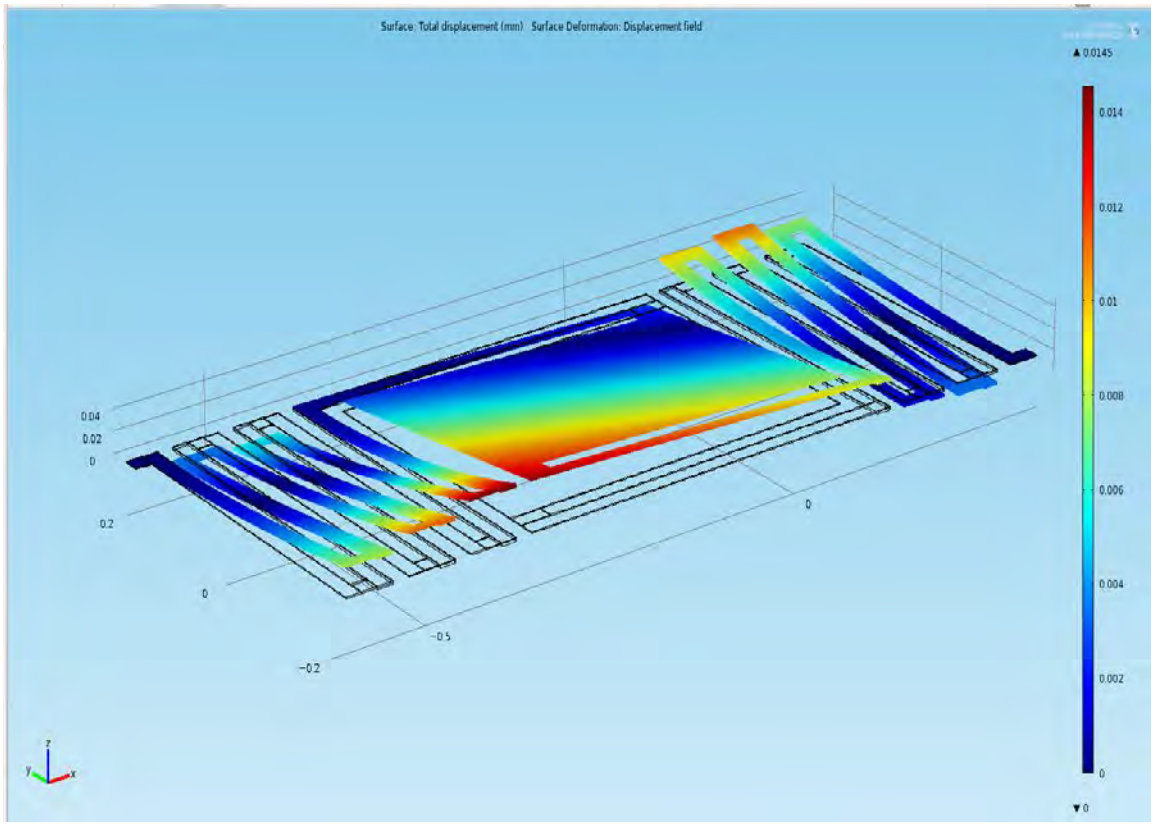

Figure 6: Initial design of solar MEMS device with Al placed toward incident solar flux on second, fourth, and sixth legs

E. FINAL DESIGN

In order to ensure the center pad successfully contacted the heat sink with as great a surface area as possible, a more creative solution was required. The solution is realized by placing the Al bimaterial beneath the piezoelectric material and shifting the bimaterial to the first, third, and fifth legs. Although this causes the bimaterial legs to bend upward toward the incident flux, the center pad actually displaces uniformly downward toward the substrate (and heat sink) as demonstrated by Figure 6. This reversal of displacement is due to the deflection angle of the final piezoelectric leg. As seen in Figure 7, utilizing a heat flux of 700 W / m^2 to simulate the solar flux on the surface of the earth with an ambient temperature of 293.15 K, the displacement of the center pad is approximately five microns, which is exactly the required displacement for the design of the device.

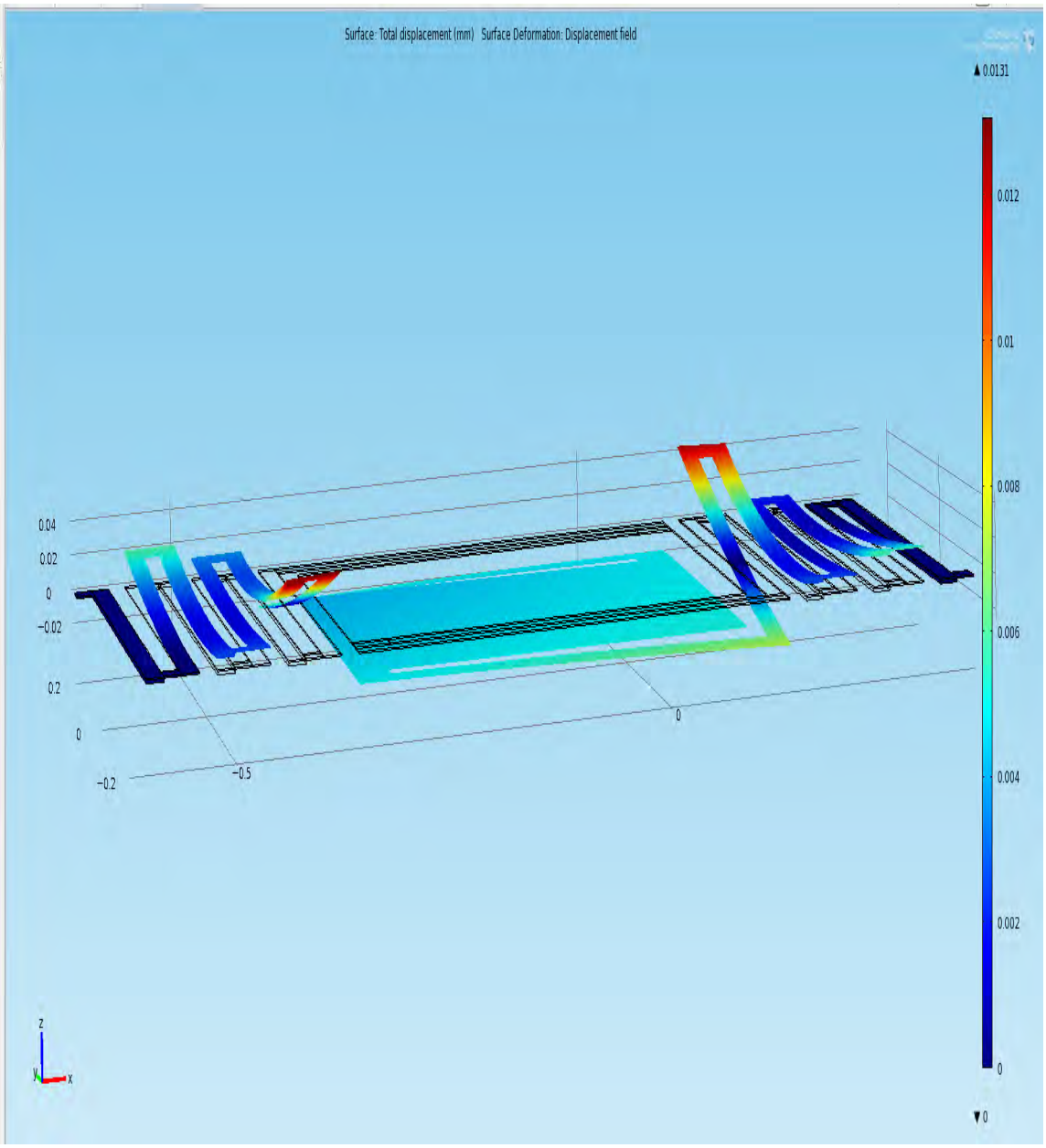

Figure 7: Solar MEMS device with Al placed away from incident solar flux on first, third, and fifth legs

V. COMSOL MULTIPHYSICS RESULTS

A. VOLTAGE GENERATION

Utilizing the piezoelectric physics model within COMSOL, the voltage created by the solar MEMS device was determined. Figure 8 shows the maximum voltage given an inbound heat flux of 700 W / m^2 with an ambient temperature of 293.15 K. The difference in electric potential, when no load is connected, is estimated at 124 V due to the displacement in Figure 7.

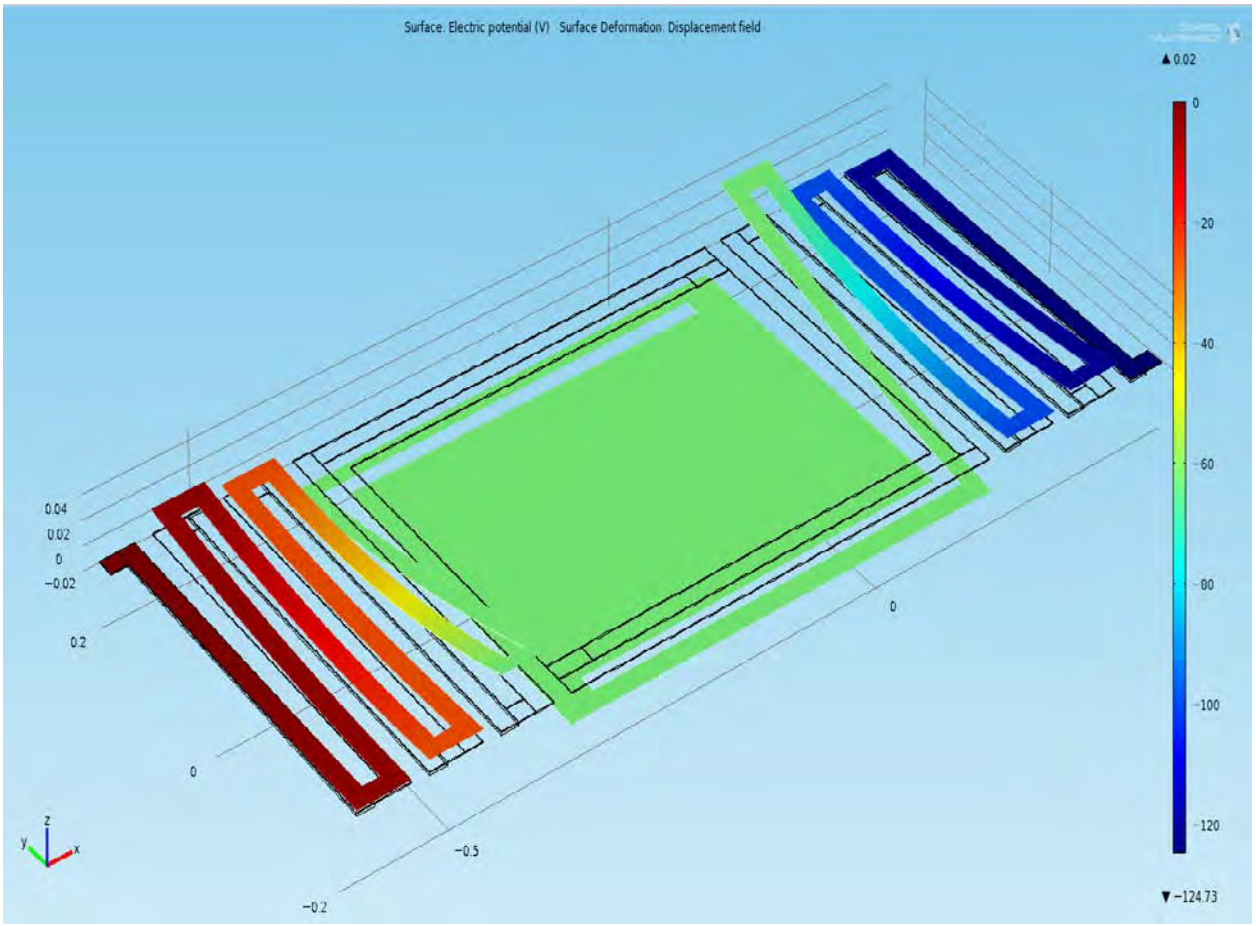

Figure 8: Maximum voltage due to maximum steady state deformation of MEMS device

B. TIME-DEPENDENT DISPLACEMENT

In order to begin to understand the time-dependent response as well as calculate the maximum efficiency of the solar MEMS device, the time to maximum displacement and temperature difference given the incident heat flux must be determined. Utilizing an inbound heat flux of 700 W/m^2 with an ambient temperature of 293.15 K, Figure's 9 and 10 display the COMSOL results when running a time-dependent solution from 0–1 seconds at 0.1 second increments. The time of maximum deflection occurs at .82 seconds coinciding with a maximum temperature of approximately 334 K.

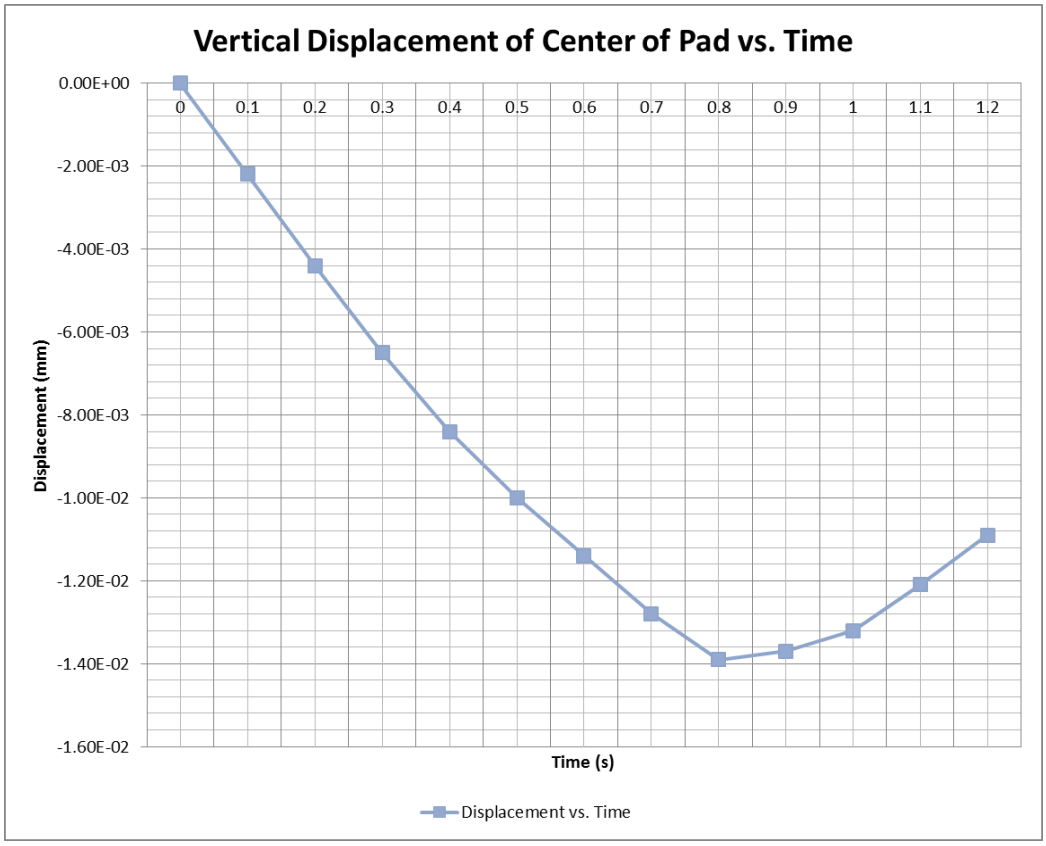

Figure 9: The vertical displacement of the solar MEMS device measured in millimeters vs. time via COMSOL multiphysics

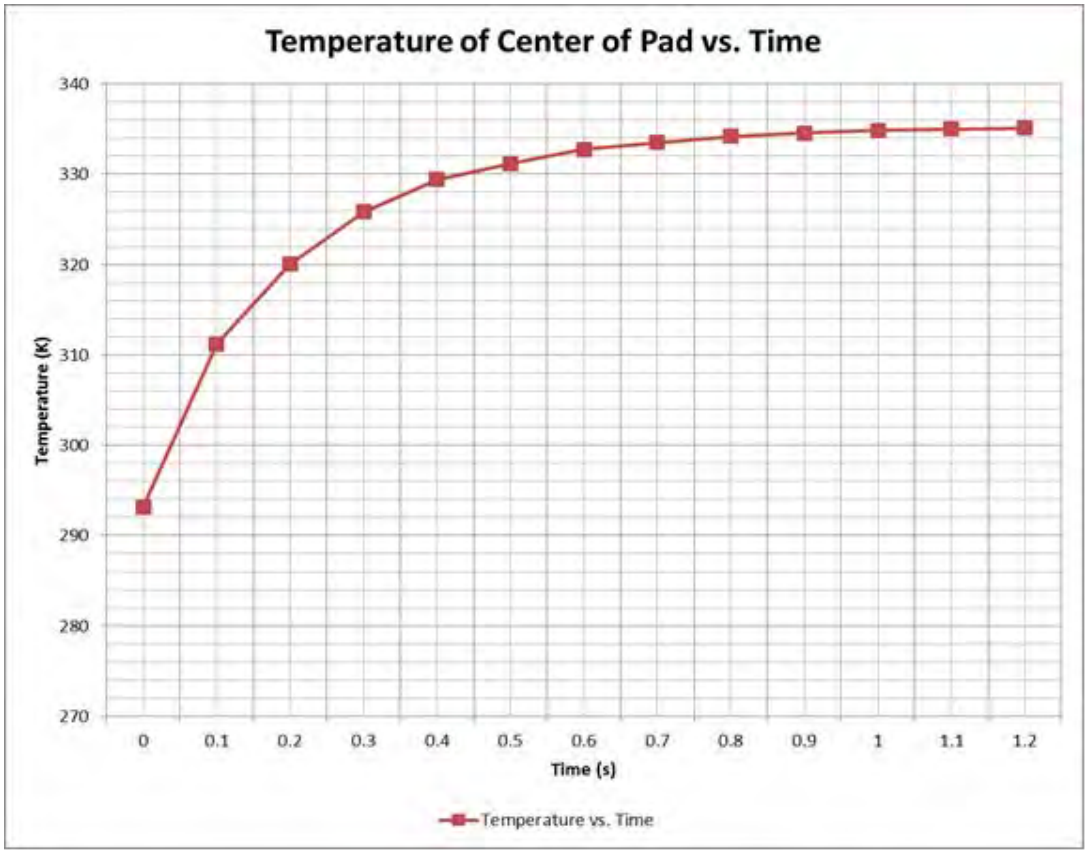

Figure 10: The temperature of the center pad of the solar MEMS device in Kelvin vs. time via COMSOL multiphysics

C. CURRENT GENERATION

A basic estimation of the current can be modeled by placing a connection between the ends of the MEMS device and completing the circuit. Figure 11 demonstrates the current density generated in a non-optimized time-dependent COMSOL model utilizing a metal connection with 24.5 Ω of resistance at a time of 1 second. Utilizing the basic equation $P=RI^2$, the instantaneous power output is 4.14 x 10^{-9} W. The model designed in Figure 5 is expected to have a larger power output due to the optimized design.

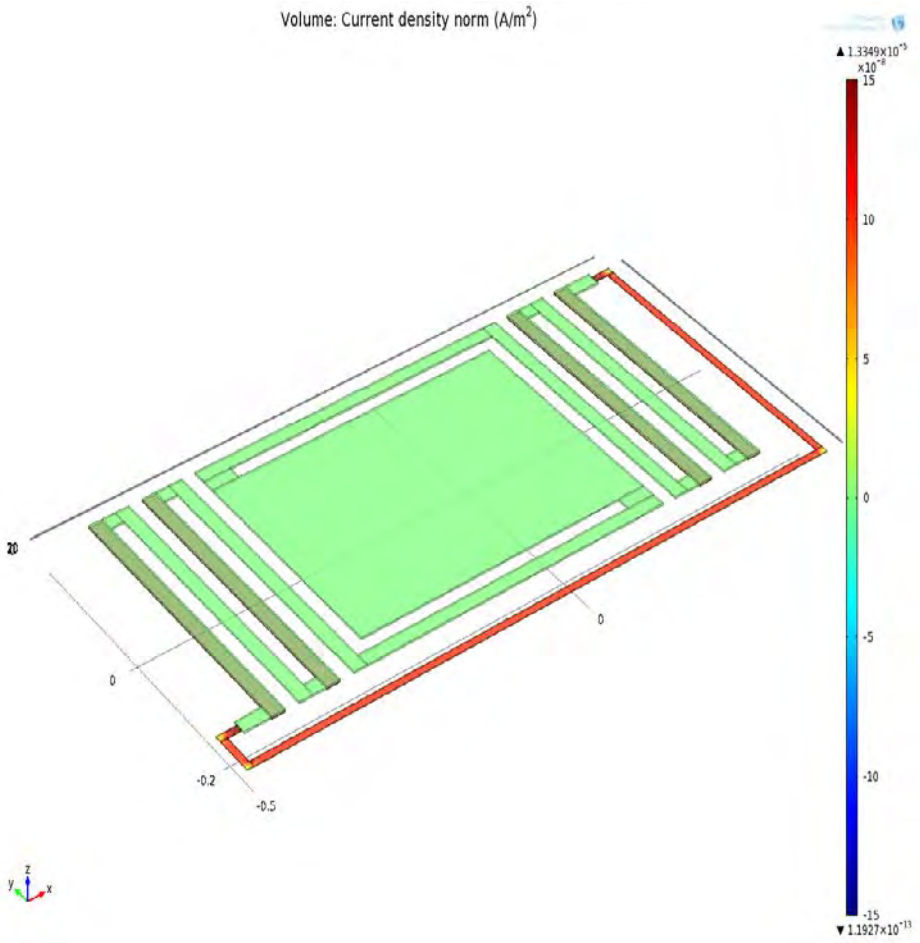

Figure 11: Instantaneous current density of a non-optimized MEMS device at time t=1 second.

VI. EFFICIENCY PREDICTIONS

A. PREDICTIONS OF THE MAXIMUM EFFICIENCY

Although actual efficiencies cannot be attained without experimental results, simple calculations allow the estimation of the possible expected efficiency. The total possible efficiency of the Solar MEMS device is the product of the maximum thermal-mechanical and piezoelectric efficiencies.

$$\eta_o = \eta_t \times \eta_p \tag{7}$$

B. THERMAL-MECHANICAL EFFICIENCY PREDICTION

As derived by Srinivasan and Spearing in [4], utilizing composite beam theory, the idea of a blocked moment, and Equation 2, the maximum work per volume accomplished in deforming the bimaterial is given by [4]:

$$W = \frac{3E_1(\Delta\alpha)^2(\Delta T)^2}{8\left(3(\lambda\xi+1)+\left(\frac{(1+\lambda\xi)^2(1+\xi^3\lambda)}{\lambda\xi(\xi+1)^2}\right)\right)\left(\frac{\xi+1}{\xi}\right)} \tag{8}$$

where E_1 equals the Young's modulus of the Al layer, $\Delta\alpha$ is the difference in the thermal expansion coefficients of the materials, ΔT is the temperature difference, λ is the ratio of Young's moduli between the two materials, and ξ is the thickness ratio between the two materials. Utilizing the values given throughout the thesis: $\Delta\alpha = 1.8\times10^{-5}K^{-1}$, ΔT = 40.85 K, $t_1 = 2\times10^{-6}$ m, $t_t = 3\times10^{-6}$ m λ =.227, and ξ=2 the work per volume done is found to be $W = 1626 J/m^3$.

Thermal-mechanical efficiencies for bimaterial actuators are time-dependent and therefore depend on the transient thermal response as well as

the activation frequency [30]. Although these can only be determined through experimental testing, the efficiency for the deformation to one maximum displacement of the MEMS device can be estimated as:

$$\eta_t = (W \times t / t_d) \Big/ S \tag{9}$$

where S is the solar flux given in Equation 1, W is the maximum work per volume in deforming the bimaterial given in Equation 8, t is the thickness of the MEMS device, and t_d is the time it takes to deform to maximum displacement. Using $W = 1626 J/m^3$, $t = 3\mu$, $t_d = .82$ seconds, and $S = 700\ W/m^2$ in Equation 9, the efficiency is $\eta_t \approx .001\%$.

C. PIEZOELECTRIC EFFICIENCY PREDICTION

The maximum efficiency for piezoelectric vibrations occurs at the natural, or resonant, frequency for the referenced material. If the alternative electromechanical coupling coefficient, given by $k_e^2 = \frac{d^2}{KC}$, approaches the value of 1 (where d is the piezoelectric coefficient given in Equation 3, K is the effective stiffness, and C is the effective capacitance), another maximum exists at a frequency given by $\Omega_{OC} = \sqrt{(1+k_e^2)} \approx \sqrt{2}$ where Ω_{OC} is the ratio of the frequency to the natural frequency [31], [32]. At these frequencies, the electromechanical efficiency is given by [33]:

$$\eta_p = \frac{1}{2}\frac{k^2}{1-k^2} \Bigg/ \left(\frac{1}{Q} + \frac{1}{2}\left(\frac{k^2}{1-k^2} \right) \right) \tag{10}$$

where η_p is the efficiency in converting mechanical energy to electrical energy, k^2 is the electromechanical coupling factor (*not* k_e), Q is the quality factor. For

AlN, $k^2 = 6.5\%$ and Q is related to the resonant frequency and damping of the MEMS structure and therefore is highly dependent on the shape of the material as well as the quality of the crystal. Q values of 5,000 are not uncommon for AlN and can be used to get an estimate of the expected efficiency [34]. Solving Equation 10, we find that $\eta_p = 99\%$.

D. RESULTS

The two maximal efficiencies display the dichotomy of the physics within the proposed solar MEMS device. The efficiencies were found given maximal work for the thermal-mechanical efficiency and oscillation at the resonant frequency for the optimized piezoelectric efficiency. Utilizing Equation 7, the gross estimate of the total efficiency is approximately 0.001%. Although this is extremely low, it should be noted that the calculation of both efficiencies can only provide gross estimations of the total efficiency and that the total efficiency may very well be greater than current single junction solar cells. Due to the innate complexity of the MEMS device, experimental results are required in order to attain actual efficiencies. However, these analytical results do point to the limiting factor in the efficiency being the thermal-mechanical efficiency. Further data analysis via actual experimental study must be conducted in order to validate these analytical results.

THIS PAGE INTENTIONALLY LEFT BLANK

VII. MICROFABRICATION PROCESS

A. GENERAL

The fabrication of the solar device will follow standard MEMS fabrication processes and is illustrated in Figure 12. First, a wafer (the substrate) will be utilized with which to grow the device on. Due to the bimaterial being on the bottom of the device, a sacrificial layer will first be deposited. After the sacrificial layer, a layer of Al will be deposited and then etched to create the alternating bottom legs of the bimaterial. The anchor holes will be etched in the sacrificial layer after that. Next, the piezoelectric material will be deposited. As stated previously, numerous methods for growth exist for both AlN and SiC on both Si and SiC. However, in this case the growth will be occurring on top of a sacrificial layer. It must be noted that the polytype of SiC grown will be dependent on the material it is grown on. For instance, in order to grow SiC on a Si substrate (or layer), single crystal 3C-SiC must be used due to the dissimilarity in crystalline structure of SiC (6H) with Si [34]. After the piezoelectric layer is successfully deposited, it will be etched into the form of the solar MEMS device. Finally, the sacrificial layer will be removed creating the freestanding solar MEMS device on top of the substrate.

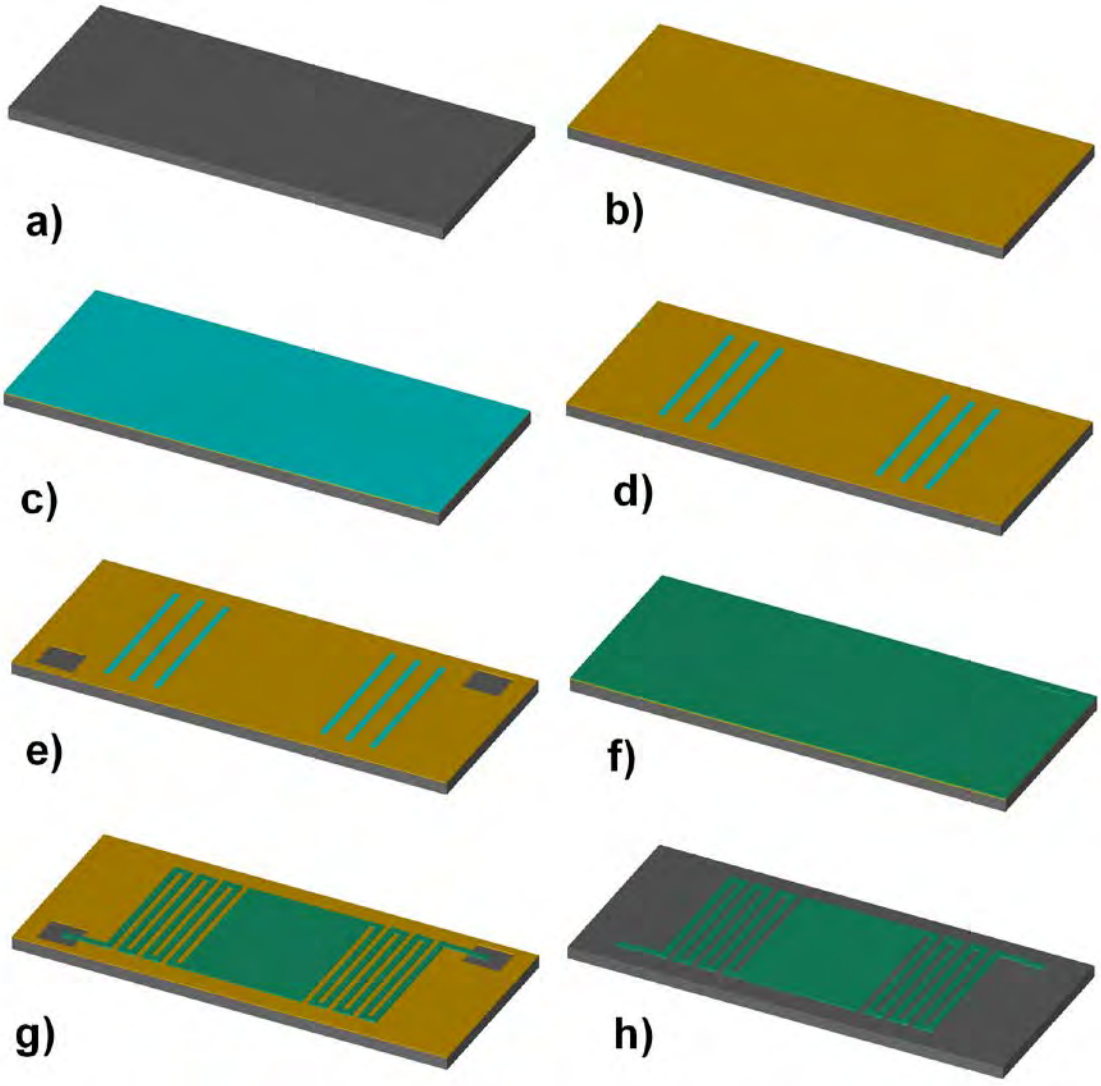

Figure 12: Microfabrication process of solar MEMS device

VIII. FUTURE WORK

A. COMPUTER MODELING

In order to maximize the efficiency, the frequency must be optimized to the natural frequency of the device. It is not currently possible to model time-dependent surface contacts between two solids in COMSOL Multiphysics. Therefore, the proper heat sink required to obtain a frequency near resonance is unknown. Additionally, since the solar heat flux will always vary, the power output of the device at different frequencies is unknown. Finally, it is unknown if the computer simulation will provide similar results to the efficiencies calculated above at resonant frequency. Further COMSOL modeling should include investigations into different resistivities in order to determine optimal power output through a time-dependent model.

B. FABRICATION

Fabrication of the AlN solar MEMS device needs to occur in order to test and evaluate both the calculated and modeled results in this thesis. It is unknown what effect different heat fluxes and heat sinks will have on the MEMS device. Sample devices must be built in order to determine the actual feasibility of the device under all solar conditions. Prior to microfabrication, investigation must continue into what sacrificial layers will be utilized. Additionally, the specific growth and etching techniques will need to be investigated prior to construction of the actual device.

THIS PAGE INTENTIONALLY LEFT BLANK

LIST OF REFERENCES

[1] Stanford University, “Stanford University Global Climate and Energy Project Technical Assessment Report,” Stanford University, 2011.

[2] Emcore Corporation, “Emcore Record Efficiency Solar Cells Released to Earth Orbit in the Final Space Shuttle Mission,” news release, Jul. 29, 2011, http://www.emcore.com/news_events/release?y=2011&news=298.

[3] L. Chang, *Foundations of MEMS*. Saddle River, NJ, Prentice Hall, 2011.

[4] P. Srinivasan and S. Mark Spearing, “Materials Selection and Design of Microelectrothermal Bimaterial Actuators,” *Journal of Microelectromechanical Systems*, vol. 16, no. 2, pp. 248–259, Apr. 2007.

[5] B. A. Blow, R. Harjani, D. L. Polla, and T. Tamagawa, “A Dual Frequency Range Integarated Circuit Accelerometer Using Capacitive and Piezoelectric Sensing Techniques,” Medtronic, Inc., Minneapolis, MN, 0–7803–1254–6/93, *IEEE*, 1993.

[6] C. V. Madhusudana and L. S. Fletcher, “Contact heat transfer-The last decade,” *AIAA Journal*, vol. 24, no. 3, pp. 510–523, Mar. 1986.

[7] National Aeronautics and Space Administration, “Temp. of Space?” Sep. 2011, http://www.nasa.gov/pdf/379068main_Temperature_of_Space.pdf.

[8] S. Trolier-Mckinstry and P. Muralt, “Thin film piezoelectrics for MEMS,” *Journal of Electroceramics*, vol. 12, pp. 7–17, 2004.

[9] B. Hwang, C. Chen, H. Lu, and T. Hsu, “Growth mechanism of reactively sputtered aluminum nitride thin films” *Materials Science and Engineering*, A325, pp. 380–388, 2002.

[10] V. Cimalla, J. Pezoldt, and O. Ambacher , “Group III nitride and SiC based MEMS and NEMS: materials properties, technology and applications,” *Journal of Physics D: Applied Physics,* vol. 40, pp. 6386–6434, 2007.

[11] C. E. Kennedy, “Review of mid-to high- temperature solar selective absorber materials,” Tech. Rep. NREL/TP-520–31267. National Renewable Energy Laboratory, Golden, CO Jul. 2002.

[12] R. Abbbott and S. Waldman, “Thermal Coatings for In-Vacuum Radiation Cooling,” Tech. Rep. LIGO-T070054–00-C, Caltech, Pasadena, CA, , Mar. 12, 2007.

[13] G. A. Slack, R. A. Tanzilli, R. O. Pohl, and J. W. Vandersande, “The Intrinsic Thermal Conductivity of AlN,” *Journal of Physics and Chemistry of Solids,* vol. 48, no. 7, pp. 641–647, 1987.

[14] N. N. Sirota, V. Z. Golodushko, “Tezisy Dokl., Vses Konf. Khi., Svyazi Poluprovdn.,” *Polumetallakh* vol. 5, pg. 98, 1974.

[15] P. Raback, “Modeling of the Sublimation Growth of Silicon Carbide Crystals,” Tech.D. Dissertation, Helsinki University of Technology, Espoo, Finland, 1999.

[16] M Syvajarvi et al., “Growth of 6H and 4H-SiC by sublimation epitaxy,” *Journal of Crystal Growth*, vol. 197, pp. 155–162, 1999.

[17] M. Scheffler and P. Colombo, *Cellular Ceramics: Structure, Manufacturing, Properties, and Applications*. Seattle, WA: Wiley, 2005.

[18] Engineering Toolbox, “Emissivity coefficients of some common materials,” Sep. 2011, http://www.engineeringtoolbox.com/emissivity-coefficients-d_447.html.

[19] M. Levinshtein, S. Rumyantsev, and M. Shur, *Properties of Advanced Semiconductor Materials: GaN, AlN, InN, BN, SiC, SiGe*. New York: John Wiley & Sons, Inc., 2001.

[20] E. L. Kern, D. W. Hamill, H. W. Deem, and H. D. Sheets, “Thermal properties of beta silicon carbide from 20 to 2000 C,” *Materials Research Bulletin*, vol. 4 S25, 1969.

[21] H. Nagasawa, K. Yagi, “3C-SiC Single Crystal Films Grown on 6-Inch Si Substrates,” Hoya Corporation, R&D Center, Tokyo, Japan, *Physica Status Solidi (b),* vol. 202, no. 335, 1997.

[22] ESPI Metals. “Aluminum Machining,” Sep. 2011, http://www.espimetals.com/index.php/technical-data/24-aluminum-machining.

[23] “Basic Mechanical and Thermal Properties of Silicon” Virginia Semicondutor, Inc., Fredericksburg, VA, 2000.

[24] S. Subrina, D. Kotchetkov, and A. Balandin, “Graphene heat spreaders for thermal management of nanoelectronic circuits,” *IEEE Electron Device Letters*, vol. 30, no. 12, pp. 1281, 2009.

[25] N. Camara et al., “Selective epitaxial growth of graphene on SiC,” *Applied Physics Letters,* vol. 93, no. 12, 2009.

[26] D. Gerlich, S. L. Dole, and G. A. Slack, “Elastic properties of aluminum nitride,” *J. Phys. Chem. Solids*, vol. 47, no. 5, pp. 437–441, 1986.

[27] K. Barbalace, “Periodic table of elements, aluminum – Al,” 1995 – 2011, http://EnvironmentalChemistry.com/yogi/periodic/Al.html.

[28] *Gmelins Handbuch der Anorganischen Chemie*, 8th edition, Silicium, Part B, Weinheim, Verlag Chemie, GmbH, 1959.

[29] F. Dong et al., “Uncooled infrared imaging device based on optimized optomechanical micro-cantilever array,” *Ultramicroscopy,* vol. 108, pp. 579–588, Mar. 26, 2007.

[30] P. Srinivasan, S. Spearing, “Effect of heat transfer on materials selection for bimaterial electrothermal actuators,” *Journal of Microelectromechanical Systems,* vol. 17, no. 3, Jun. 2008.

[31] N. duToit, B. Wardle, S. Kim, “Design considerations for MEMS-scale piezoelectric mechanical vibration energy harvesters,” *Integrated Ferroelectrics*, vol. 71, pp. 121–160, 2005.

[32] Y. C. Shu, I. C. Lien, “Efficiency of energy conversion for a piezoelectric power harvesting system.” *Journal of Micromechanics and Microengineering*, vol. 16, pp. 2429–2438, 2006.

[33] C. D. Richards, M. J. Anderson, D. F. Bahr, and R. F. Richards, “Efficiency of energy conversion for devices containing a piezoelectric component,” *Journal of Micromechanics and Microengineering*, vol. 14, p. 717, 2004.

[34] A. N. Cleland, M. Pophristic, and I. Ferguson, “Single-crystal Aluminum Nitride Nanomechanical Resonators,” *Applied Physics Letters,* vol. 79, no. 13, 2001.

[35] W. Choyke, H. Matsunami, and G. Pensl, *Silicon Carbide: Recent Major Advances*. Berlin, Germany: Springer, 2004.

THIS PAGE INTENTIONALLY LEFT BLANK

INITIAL DISTRIBUTION LIST

1. Defense Technical Information Center
   Ft. Belvoir, Virginia

2. Dudley Knox Library
   Naval Postgraduate School
   Monterey, California